antioxidants

MDPI

*Article*

# Dual Mechanisms of Cardiac Action Potential Prolongation by 4-Oxo-Nonenal Increasing the Risk of Arrhythmia; Late $Na^+$ Current Induction and hERG $K^+$ Channel Inhibition

**Seong-Woo Choi [1], Ming-Zhe Yin [2,3], Na-Kyeong Park [2], Joo-Han Woo [1] and Sung-Joon Kim [2,*]**

[1] Department of Physiology, Dongguk University College of Medicine, Gyeongju 38066, Korea; physiolcsw@dongguk.ac.kr (S.-W.C.); gabriel929@dongguk.ac.kr (J.-H.W.)
[2] Department of Physiology, Seoul National University College of Medicine, Seoul 03080, Korea; myungchul5_5@snu.ac.kr (M.-Z.Y.); pnk96@snu.ac.kr (N.-K.P.)
[3] Department of Anesthesiology, Second Affiliated Hospital of Zhejiang University School of Medicine, Hangzhou 310058, China
* Correspondence: physiolksj@gmail.com or sjoonkim@snu.ac.kr; Tel.: +82-2-740-8230

**Abstract:** 4-Oxo-nonenal (4-ONE) is an endogenous lipid peroxidation product that is more reactive than 4-hydroxy-nonenal (4-HNE). We previously reported the arrhythmic potential of 4-HNE by suppression of cardiac human Ether-a-go-go Related Gene (hERG) $K^+$ channels with prolonged action potential duration (APD) in cardiomyocytes. Here, we illustrate the higher arrhythmic risk of 4-ONE by modulating the cardiac $hNa_V1.5$ channel currents ($I_{NaV}$). Although the peak amplitude of $I_{NaV}$ was not significantly changed by 4-ONE up to 10 μM, the rate of $I_{NaV}$ inactivation was slowed, and the late $Na^+$ current ($I_{NaL}$) became larger by 10 μM 4-ONE. The chemical modification of specific residues in $hNa_V1.5$ by 4-ONE was identified using MS-fingerprinting analysis. In addition to the changes in $I_{NaV}$, 4-ONE decreased the delayed rectifier $K^+$ channel currents including the hERG current. The L-type $Ca^{2+}$ channel current was decreased, whereas its inactivation was slowed by 4-ONE. The APD prolongation by 10 μM of 4-ONE was more prominent than that by 100 μM of 4-HNE. In the computational in silico cardiomyocyte simulation analysis, the changes of $I_{NaL}$ by 4-ONE significantly exacerbated the risk of arrhythmia exhibited by the TdP marker, qNet. Our study suggests an arrhythmogenic effect of 4-ONE on cardiac ion channels, especially $hNa_V1.5$.

**Keywords:** lipid peroxidation; 4-oxo-nonenal; heart; arrhythmia; late $Na^+$ current



**Citation:** Choi, S.-W.; Yin, M.-Z.; Park, N.-K.; Woo, J.-H.; Kim, S.-J. Dual Mechanisms of Cardiac Action Potential Prolongation by 4-Oxo-Nonenal Increasing the Risk of Arrhythmia; Late $Na^+$ Current Induction and hERG $K^+$ Channel Inhibition. *Antioxidants* **2021**, *10*, 1139. https://doi.org/10.3390/antiox10071139

Academic Editors: Stefania Pizzimenti, Giuliana Muzio and Giuseppina Barrera

Received: 22 June 2021
Accepted: 15 July 2021
Published: 19 July 2021



## 1. Introduction

Reactive carbonyl species (RCS), such as 4-hydroxy-nonenal (4-HNE) and 4-oxo-nonenal (4-ONE), are secondary peroxidation products of unsaturated fatty acids [1,2]. The ability of RCS to covalently react with the nucleophilic groups of nucleic acids and proteins exerts various pathophysiological consequences [3–8]. The heart is vulnerable to reactive oxygen species (ROS) and RCS produced by oxidative damage in ischemia/reperfusion, fibrillation, and heart failure [9–12]. Despite the importance of altered ion channel functions in cardiac diseases, the pathophysiological plausibility of interactions between ion channels and RCS has rarely been investigated.

We previously reported that 4-HNE has a potential arrhythmic effect on the heart by extending the action potential duration (APD), which was mediated by the inhibition of human Ether-a-go-go Related Gene (hERG) $K^+$ channel current ($I_{Kr}$) [13]. In addition to the voltage-gated $K^+$ channels, such as hERG, various functional disturbances of the human cardiac $Na^+$ channel ($hNa_V1.5$) are associated with an increased risk of arrhythmia [14]. The *SCN5A* gene encodes the $hNa_V1.5$ α-subunit, and mutations in *SCN5A* are associated with inherited susceptibility to ventricular arrhythmia, such as Brugada syndrome, long QT syndrome class 3 (LQT-3), or atrial fibrillation [15,16].

A gain-of-function mutation of *SCN5A* leads to increased $Na^+$ influx during systole, resulting in delayed action potential repolarization or early afterdepolarization (EAD) of the cardiac AP [16]. Specifically, the persistent or non-inactivating component of $hNa_V1.5$, called the late $Na^+$ current ($I_{NaL}$), could be responsible for the prolonged APD of LQT-3. However, the chemical modification of $hNa_V1.5$ and its arrhythmogenic effect, such as $I_{NaL}$ induction, has been rarely investigated. Interestingly, previous studies have shown that the oxidative condition of cardiac ischemia and heart failure enhanced $I_{NaL}$ [17–19]. The plausible changes of $hNa_V1.5$ current ($I_{NaV}$) and the putative induction of $I_{NaL}$ in ROS-mediated arrhythmia attracted us to investigate the modification of $hNa_V1.5$ activity by RCS.

In the present study, we highlighted the arrhythmic potentials of 4-ONE, which is formed from 4-hydroperoxy-2-nonenal, the same precursor as 4-HNE [1]. Structurally, 4-ONE differs at the C4 position with a ketone group instead of the hydroxyl group of 4-HNE, increasing the electrophilic reactivity of 4-ONE. Therefore, 4-ONE modifies various nucleophilic amino acids, such as cysteine (Cys), lysine (Lys), histidine (His), and arginine (Arg) [20–22]. However, a previous study on the effects of 4-ONE on ion channel activity was limited to TRPA1 and TRPV1 nonselective cation channels as the harmful sensory signals [23]. In addition to $hNa_V1.5$, we also examined the effects of 4-ONE on hERG ($I_{Kr}$), *KCNQ1/KCNE1* ($I_{Ks}$), and L-type voltage-operated $Ca^{2+}$ channels ($I_{Ca,L}$). Finally, the relative contribution of the $I_{NaV}$ modulation to APD prolongation and arrhythmogenic risk was analyzed by a recently announced method of proarrhythmic risk analysis called Comprehensive in vitro Proarrhythmia Assay (CiPA), cooperatively using experimental data and in silico simulation [24,25].

## 2. Materials and Methods

### 2.1. Cell Preparation

HEK-293 cell line cells stably overexpressing $hNa_V1.5$ ($hNa_V1.5$-HEK cell) or hERG1a (hERG-HEK cell) were used for the electrophysiological recording of $I_{NaV}$ and $I_{Kr}$, respectively. The $hNa_V1.5$-HEK cell was kindly donated by Dr. Jae-Hong Ko (Chung-Ang University, Seoul, Korea). The $hNa_V1.5$-HEK cells were maintained in DMEM (Thermo Fisher Scientific, Bremen, Germany) supplemented with 10% FBS (Serana Europe, Pessin, Germany) and geneticin G418 (Sigma-Aldrich, Saint Louis, MO, USA). The hERG-HEK cell was kindly donated by Dr. Han Choe (University of Ulsan, Seoul, Korea). The hERG-HEK cells were maintained in MEM (Thermo Fisher Scientific) supplemented with 10% FBS. To record the slowly activating voltage-dependent $K^+$ current ($I_{Ks}$), HEK cells were transiently overexpressed with *KCNQ1* and *KCNE1* plasmid DNA (RG219869 and RC225088, OriGene Technologies, Rockville, MD, USA) using FuGENE 6 kit (Roche, Penzberg, Germany). To record L-type $Ca^{2+}$ current ($I_{Ca,L}$) and cardiac action potential (AP), guinea-pig ventricular myocytes (GPVMs) were isolated using the Langendorff apparatus as described previously [13].

### 2.2. Electrophysiological Recording

Conventional whole-cell voltage and current-clamp were conducted for currents and AP recordings, respectively. For the $I_{NaV}$ recording, high giga-seal resistance (>2 GΩ), low series resistance (<10 MΩ), and the series resistance compensation (80%) were introduced to reduce voltage-clamp error. The extracellular bath solution for the $I_{NaV}$ and $I_{NaL}$ recordings in $hNa_V1.5$-HEK cells contained 130 mM NaCl, 10 mM HEPES (4-(2-hydroxyethyl)-1-piperazineethanesulfonic acid), 4 mM CsCl, 1 mM $MgCl_2$, 2 mM $CaCl_2$, and 10 mM glucose adjusted to pH 7.4 with NaOH. The intracellular pipette solution for the $I_{NaV}$ and $I_{NaL}$ recordings contained 117 mM CsCl, 20 mM NaCl, 1 mM $MgCl_2$, 5 mM HEPES, 5 mM EGTA, 5 mM MgATP, and 0.4 mM TrisGTP adjusted to pH 7.3 with CsOH. The extracellular bath solution for the $I_{Kr}$ and $I_{Ks}$ recordings contained 145 mM NaCl, 3.6 mM KCl, 10 mM HEPES, 1 mM $MgCl_2$, 1.3 mM $CaCl_2$, and 5 mM glucose adjusted to pH 7.4 with NaOH. The intracellular pipette solution for the $I_{Kr}$ and $I_{Ks}$ recordings contained 100 mM K-aspartate,

25 mM KCl, 5 mM NaCl, 10 mM HEPES, 1 mM $MgCl_2$, 4 mM MgATP, and 10 mM BAPTA adjusted to pH 7.25 with KOH. The extracellular bath solution for $I_{Ca,L}$ contained 145 mM CsCl, 10 mM HEPES, 1 mM $MgCl_2$, 1.8 mM $CaCl_2$, and 5 mM glucose adjusted to pH 7.4 with CsOH. The intracellular pipette solution for $I_{Ca,L}$ contained 106 mM CsCl, 20 mM TEA-Cl, 5 mM NaCl, 10 mM HEPES, 5 mM MgATP, and 10 mM EGTA adjusted to pH 7.25 with CsOH. The compositions of the extracellular solutions used for the AP recording contained 145 mM NaCl, 5.4 mM KCl, 10 mM HEPES, 1 mM $MgCl_2$, 1.8 mM $CaCl_2$, and 5 mM glucose adjusted to pH 7.4 with NaOH. The intracellular solution contained 120 mM K-aspartate, 20 mM KCl, 5 mM NaCl, 2 mM $CaCl_2$, 5 mM EGTA, 10 mM HEPES, and 5 mM MgATP adjusted to pH 7.25 with KOH.

### 2.3. In Silico Simulation

CiPAORdv1.0 (modified O'Hara–Rudy model) was used to simulate human ventricular AP and its changes due to the altered ionic currents ($I_{Kr}$, $I_{Ks}$, $I_{Ca,L}$, $I_{NaV}$, and $I_{NaL}$) by 4-ONE and 4-HNE. The levels of ionic current inhibition and the equations of inactivation time constant obtained from the experimental results are presented in Table 1.

**Table 1.** The input values for the simulation of AP using CiPAORdv1.0.

| | Control | 4-HNE | 4-ONE |
|---|---|---|---|
| ths ($I_{Nav}$) | $\frac{1.0}{0.009794e^{-\frac{v+17.95}{28.05}} + 0.3343e^{\frac{v+5.730}{56.66}}}$ | | $\frac{1.0}{0.0036794e^{-\frac{v+17.95}{28.05}} + 0.3343e^{\frac{v+5.730}{56.66}}}$ |
| thL ($I_{NaL}$) | 200.0 | | 400.0 |
| tfcaf ($I_{Ca,L}$) | $7.0 + \frac{1.0}{0.04e^{-\frac{v-4.0}{7.0}} + 0.04e^{\frac{v-4.0}{7.0}}}$ | | $7.0 + \frac{1.0}{0.04e^{-\frac{v-10.0}{7.0}} + 0.04e^{\frac{v-10.0}{7.0}}}$ |
| tfcas ($I_{Ca,L}$) | $100.0 + \frac{1.0}{0.00012e^{-\frac{v}{3.0}} + 0.00012e^{\frac{v}{7.0}}}$ | | $100.0 + \frac{1.0}{0.00006e^{-\frac{v-10}{3.0}} + 0.00006e^{\frac{v-10}{7.0}}}$ |
| Conductance for $I_{Kr}$ | 1.0 | 0.6 | 0.4 |
| Conductance for $I_{Ks}$ | 1.0 | 0.8 | 0.7 |
| Conductance for $I_{Ca,L}$ | 1.0 | 1.0 | 0.6 |

### 2.4. Tandem Mass Spectrometry

The total lysates of the $hNa_V1.5$-HEK cells treated with 4-ONE (10 μM) were subjected to SDS-PAGE for mass spectrometry (MS). The $hNa_V1.5$ bands were cut from the SDS-PAGE gel and digested in gel with trypsin (Promega, Madison, WI, USA). The subsequent procedures were similar to the previous MS [13]. A fragment mass tolerance of 1.0 Da, peptide mass tolerance of 25 ppm, and maximum missed cleavage of 2 were set. The result filters were performed with charge states versus scores (XCorr by Sequest) where the minimal scores for the charge states were +1: 1.6, +2: 1.7, +3: 3.0, and >+4: 3.5. The carbamidomethylation (+57.021 Da) of cysteine (C) was set as a static modification, and the following variable modifications were allowed: Michael addition, +154 Da (C, H, K, R); Schiff base addition, +136 Da (C, H, K); and oxidation, +15.995 Da (M). The respective data for the post-translational modification (PTM) sites by 4-ONE were transformed and analyzed with Scaffold 4 program (Proteome Software, Portland, OR, USA).

### 2.5. Chemicals

The compounds 4-ONE and 4-HNE were purchased from Cayman Chemical (Ann Arbor, MI, USA). The 4-ONE and 4-HNE were stored in 20 mM stocks in DMSO at −20 °C. Immediately prior to the application to the cells, 4-ONE and 4-HNE were freshly diluted with extracellular bath solution to the final target concentrations. Application of 4-ONE and 4-HNE was processed for at least 5 min to obtain stable electrophysiological responses. Other chemicals were purchased from Sigma-Aldrich (St. Louis, MO, USA).

### 2.6. Statistical Analysis

Data are expressed as mean ± S.E., and the statistical analyses were determined using paired or unpaired Student's *t*-tests. A $p$-value < 0.05 was considered as statistically significant.

## 3. Results

### 3.1. Slowed $hNa_V1.5$ Inactivation and $I_{NaL}$ Induction by 4-ONE

The effect of 4-ONE on cardiac $hNa_V1.5$ was evaluated using stably overexpressing $hNa_V1.5$ in the HEK-293 cell line ($hNa_V1.5$-HEK cell). In the whole-cell voltage-clamp condition, the inward $I_{NaV}$ was recorded by applying −40 mV of depolarization pulse (300 ms) from −120 mV holding potential. After confirming the stable recording of $I_{NaV}$, 4-ONE was applied to the bath perfusing solution, which reduced the peak amplitude of $I_{NaV}$ in a dose-dependent manner (Figure 1A; remaining current after 4-ONE treatment: 94.25% for 1 μM, 88.22% for 10 μM, 72.53% for 30 μM, and 63.66% for 60 μM 4-ONE; $n$ = 3, $n$ = 6, $n$ = 3, and $n$ = 3;, respectively). The reduced $I_{NaV}$ was not restored by washing 4-ONE (data not shown), which was similar to the irreversible effect of 4-HNE on $I_{hERG}$, as previously reported [13]. It has been reported that the in vivo concentration of 4-HNE under pathophysiological conditions ranges 1–100 μM [1]. In contrast, the in vivo concentration of 4-ONE has not been reported. However, an experiment on EA.hy 926 endothelial cells treated with ferrous sulfate suggested that the endogenous concentration of 4-ONE could be increased to 20 μM [26]. Therefore, we applied 10 μM 4-ONE in the subsequent experiments.

The current–voltage (I–V) relationship curves of the $I_{NaV}$ showed a minute decrease in the peak amplitude at 10 μM 4-ONE (Figure 1C; peak inward current at −40 mV of −1071.8 ± 84.17 and −972.3 ± 85.52 pA/pF for control and 4-ONE, respectively, $n$ = 6), whereas 4-HNE had no significant effect even at 100 μM (Figure 1B). The I–V curves were converted to the conductance–voltage (G–V) curve for analyzing the voltage dependence of $hNa_V1.5$, which showed a slight left-shift, indicating that 4-ONE could reduce the threshold of activation (Figure 1E; half-maximal voltage of activation of −53.7 and −56.3 mV for control and 4-ONE, respectively, $n$ = 6). The steady-state inactivation property of $hNa_V1.5$ was analyzed by using the double pulse protocol (Figure 1D, inset). The steady-state inactivation curve also showed a slight left-shift by 4-ONE (Figure 1D; half-maximal voltage of inactivation of −74.5 and −77.5 mV for control and 4-ONE, respectively, $n$ = 6).

Upon analysis of the inactivation speed of $I_{NaV}$, the rate of inactivation that was slowed by 4-ONE (Figure 2A, left) was notable. When the normalized decaying components of $I_{NaV}$ were fit to a double exponential equation, both time constants for the fast and the slow components ($\tau_{fast}$ and $\tau_{slow}$) were increased by 4-ONE (Figure 2A, right). The delayed inactivation of $I_{NaV}$ suggested an increase in $I_{NaL,}$ which is the residual activity of $hNa_V1.5$ that was flowing after the large peak $Na^+$ current during AP. To analyze $I_{NaL}$ more specifically, we applied the AP-like voltage-clamp protocol, two-step depolarization followed by a reverse-ramp voltage pulse (Figure 2B, upper gray line). The resurgent inward current during the reverse-ramp period reflected the augmented $I_{NaL}$ by 4-ONE (Figure 2B, b; current density of −2.79 ± 0.27 and −5.16 ± 0.53 pA/pF for control and 4-ONE, respectively, $n$ = 13). The sustained current at 50 ms after the peak $Na^+$ influx was increased as well (Figure 2B, a; current density of −3.44 ± 0.56 and −8.99 ± 0.96 pA/pF for control and 4-ONE, respectively, $n$ = 13). The increased inward currents (a and b) in the presence of 4-ONE were reversed by additional application of 50 μM of ranolazine, a late $Na^+$ current inhibitor (Figure 2B, −5.50 ± 1.04 and −3.14 ± 0.60 pA/pF, a and b, respectively, $n$ = 6). In contrast to the significant induction of $I_{NaL}$ by 10 μM 4-ONE, the application of 100 μM 4-HNE induced neither slower inactivation nor $I_{NaL}$ (Figure 2C,D).

The effects of 4-ONE on $I_{NaV}$ could be due to the PTM of $hNa_V1.5$, i.e., direct binding of 4-ONE with nucleophilic amino acids, such as Cys, His, Lys, and Arg [20,27]. The tandem MS of $hNa_V1.5$ with or without 4-ONE treatment revealed four different sites of modification: $His^{445}$, $His^{472}$, $Lys^{496}$, and $Arg^{878}$. The representative MS/MS spectrum for the peptides $^{443}$KEhEALTIR$^{451}$, $^{459}$SSLEMSPLAPVNShER$^{474}$, and $^{481}$RmSSGTEECGEDRLPk$^{496}$

shows that His$^{445}$, His$^{472}$, and Lys$^{496}$ were commonly modified with Schiff base addition (Figure 3A–C). Another spectrum shows the Michael addition of Arg$^{878}$ in the peptide $^{864}$NYSELRDSDSGLLPr$^{878}$ (Figure 3D). The 4-ONE-binding sites were visualized with the schematic topology of the hNa$_V$1.5 channel (Figure 3E). The sites of the Schiff base addition were located at the intracellular linker between domain I (DI) and domain II (DII). The site of the Michael addition was located at the extracellular S5–S6 linker of DII.

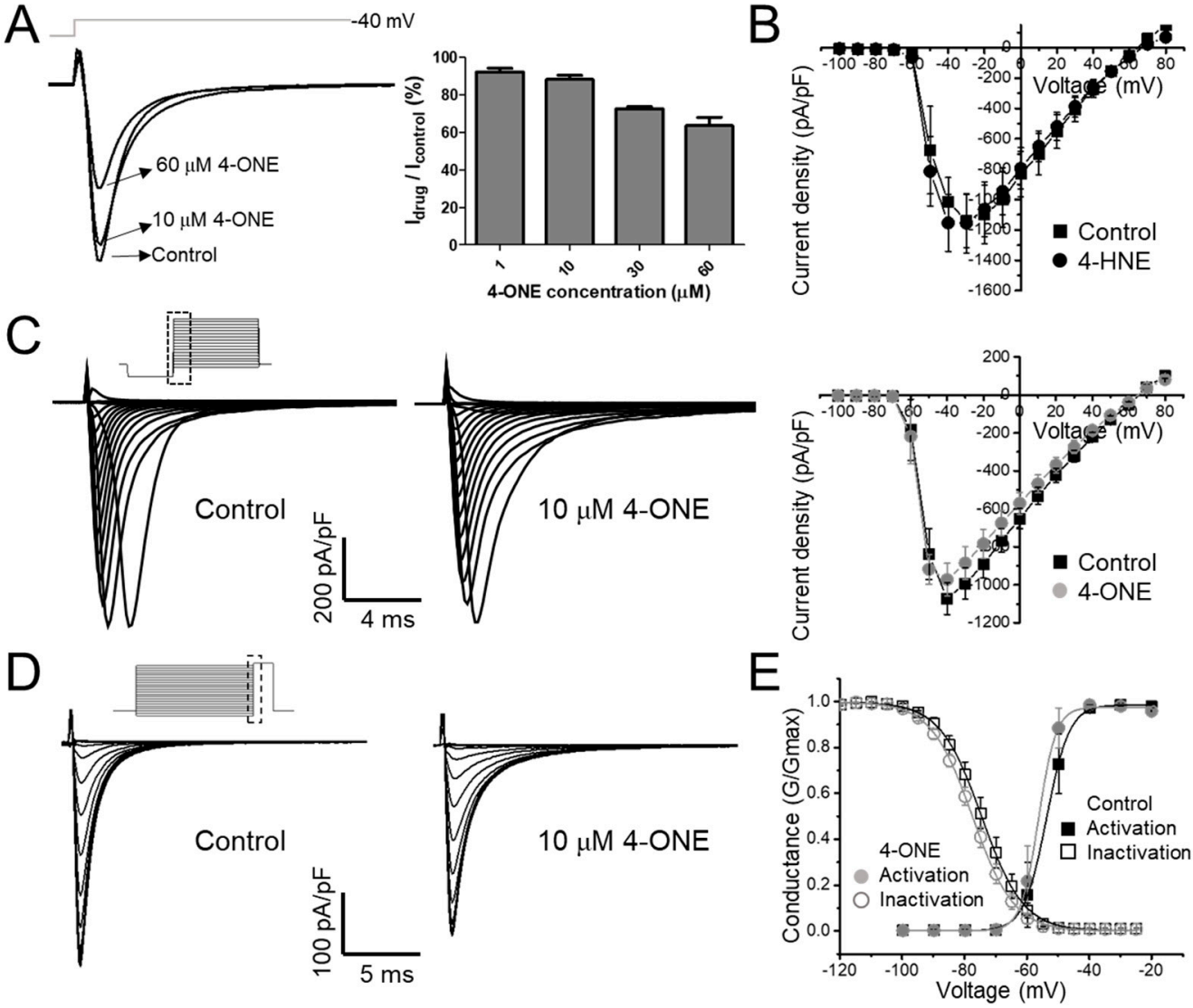


**Figure 1.** The modulations of hNa$_V$1.5 channel by 4-oxo-nonenal (4-ONE) were evaluated in HEK-293 cell line cells stably overexpressing hNa$_V$1.5 (hNa$_V$1.5-HEK cell). (**A**) The Na$_V$1.5 current ($I_{NaV}$) was activated by applying a depolarization pulse to −40 mV from −120 mV of hyperpolarized potential. (**B**,**C**) The current–voltage (I–V) relationship was analyzed by applying multistep depolarization pulse protocol from −100 to 80 mV from −120 mV of hyperpolarization for 200 ms. (**B**) I–V relationship for control and 100 μM 4-hydroxy-nonenal (4-HNE)-treated $I_{NaV}$. (**C**) Raw traces and I–V relationship of $I_{NaV}$ for control and 10 μM 4-ONE. (**D**) Steady-state inactivation of $I_{NaV}$ was analyzed at −20 mV by applying 200 ms of pre-inactivating voltages from −120 to −25 mV. (**E**) Relative conductance of inactivation and activation voltage dependences was analyzed by 10 μM 4-ONE applications.

### *3.2. Multiple Effects of 4-ONE on $I_{Kr}$, $I_{Ks}$, and $I_{Ca,L}$*

The effects of 4-ONE on cardiac $K^+$ channels were evaluated using the hERG and *KCNQ1/KCNE1* expressing HEK-293 cells. The acute treatment of 10 μM of 4-ONE reduced the peak amplitudes of $I_{Kr}$ (hERG $K^+$ current) and $I_{Ks}$ (*KCNQ1/KCNE1* current) by 65% (Figure 4A; peak current density of 73.91 ± 7.55 and 25.93 ± 5.32 pA/pF at 20 mV for control

and 4-ONE, respectively, $n$ = 8) and 29%, respectively (Figure 4B; peak current density of 35.37 ± 8.95 and 25.66 ± 5.39 pA/pF at 40 mV for control and 4-ONE, respectively, $n$ = 6). The cardiac $I_{Ca,L}$ was recorded from GPVMs. The peak amplitude of $I_{Ca,L}$ was decreased by 45% (Figure 4C; peak inward current at 0 mV of −4.30 ± 0.29 and −2.36 ± 0.36 pA/pF for control and 4-ONE, respectively, $n$ = 5). It was notable that 4-ONE also slowed the inactivation of $I_{Ca,L}$ (Figure 4D). When the inactivation phase of $I_{Ca,L}$ was fit to double exponential function, the slow component of time constant ($\tau_{slow}$) became larger by 4-ONE at 0 and 10 mV (Figure 4D; $\tau_{slow}$ at 0 mV of 122.8 ± 11.68 and 145.9 ± 10.94 ms and $\tau_{slow}$ at 10 mV of 126.1 ± 9.92 and 144.3 ± 2.77 ms for control and 4-ONE, respectively, $n$ = 7).

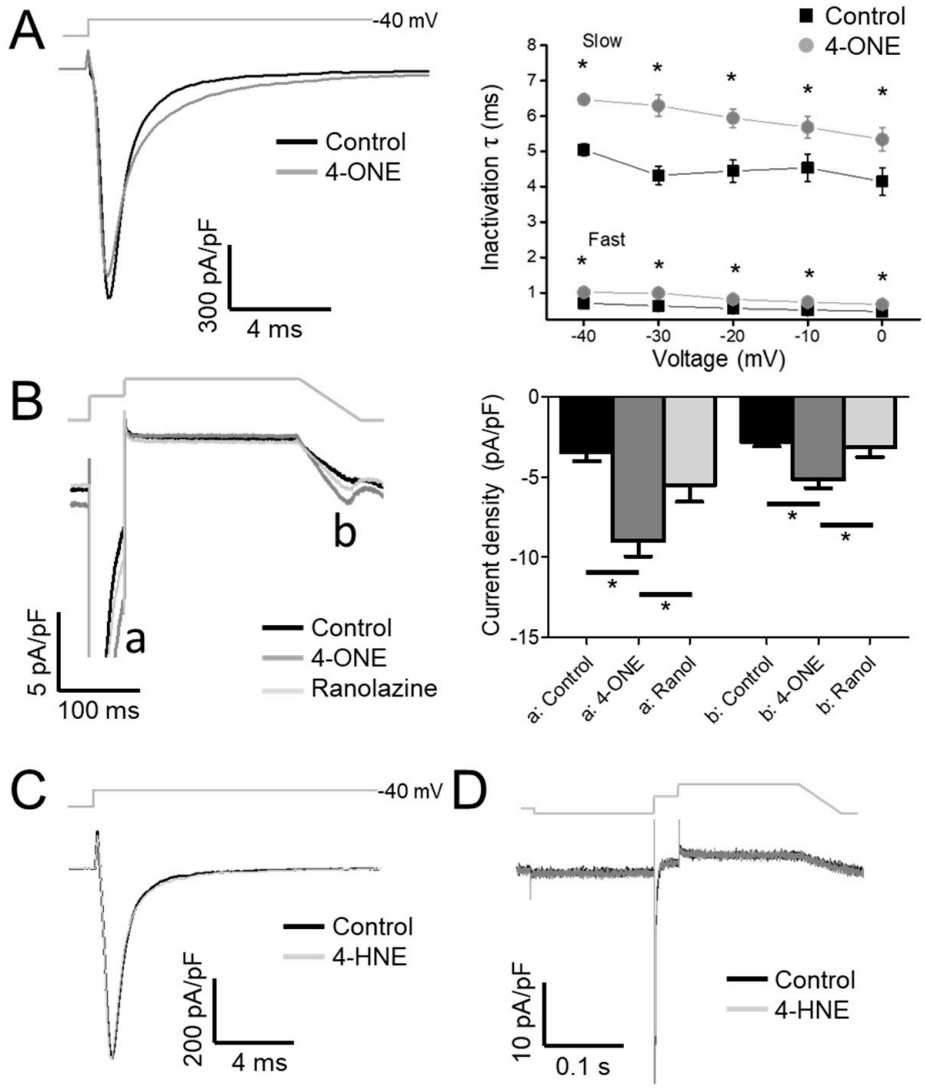


**Figure 2.** The inactivation decay of $I_{NaV}$ and the late $Na^+$ current ($I_{NaL}$) by 4-ONE were analyzed. (**A**) $I_{NaV}$ was activated by applying depolarization pulses (−40, −30, −20, −10, and 0 mV) from −120 mV of holding potential. The current decay was analyzed using double exponential fitting. (**B**) $I_{NaL}$ through $hNa_V1.5$ channel was recorded by applying action potential-like repolarization pulse protocol. The $I_{NaV}$ was activated by short depolarization to −20 mV from −120 mV of hyperpolarized potential (a). The resurgent $I_{NaL}$ was then recorded during ramp pulse repolarization (b). (**C**,**D**) 4-HNE treatment induced neither the inactivation decay of $I_{NaV}$ nor the $I_{NaL}$. All the data were analyzed using paired $t$-tests, where a $p < 0.05$ was considered statistically significant (*).

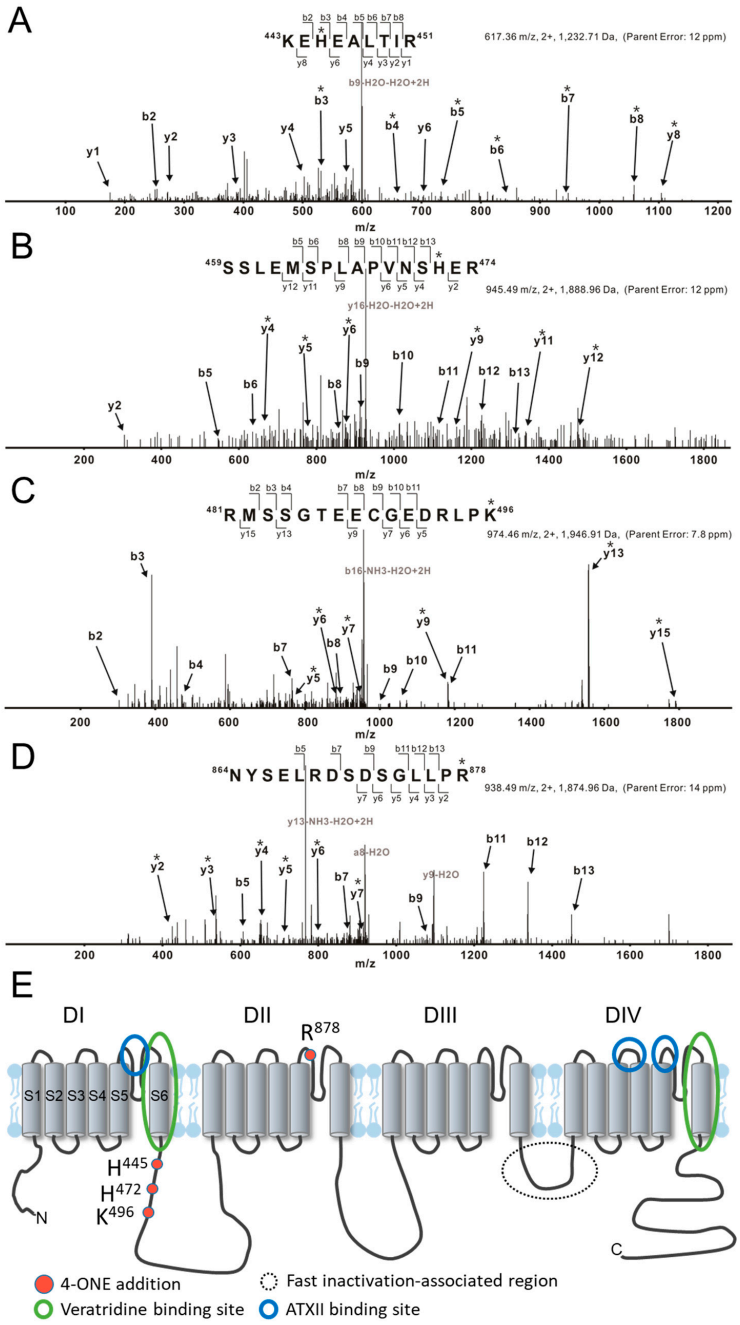


**Figure 3.** LC/MS/MS CID mass spectra of 4-ONE-modified hNa$_V$1.5 peptides. (**A**–**D**) Tryptically digested peptides are fragmented to KEhEALTIR, SSLEMSPLAPVNShER, RmSSGTEECGEDRLPk, and NYSELRDSDSGLLPr, respectively. The sites of the 4-ONE Schiff base addition (**A**–**C**) or Michael addition (**D**) are localized to His$^{445}$, His$^{472}$, Lys$^{496}$, and Arg$^{878}$ by analysis of b and y ion fragmentation patterns. The product ions containing 4-ONE addition are indicated with asterisks (*). (**A**) The mass addition of 136 to the b and y ions containing His$^{445}$, including y8 and b3–b8, combined with the absence of this addition to y1–y4, y6, and b2 identifies His$^{445}$ as the 4-ONE-modified amino acid. (**B**) Ions b5, b6, b8–b13, and y2 lack the addition of 136 Da that is present on ions y4–y6, y9, y11, and y12, thus localizing the Schiff base adduct to His$^{472}$. (**C**) Ions b2–b4 and b7–b11 lack the addition of 136 Da that is present on ions y5–y7, y9, y13, and y15 (Lys$^{496}$). (**D**) Ions b5, b7, b9, and b11–b13 lack the addition of 154 Da and ions containing Arg$^{878}$ show the addition (y2–y7). (**E**) The topological structure of hNa$_V$1.5, including 4-ONE addition amino acids and binding sites. The previously known binding regions of $I_{NaL}$ activators veratridine and *Anemonia viridis* toxin 2 are marked with blue and green circles, respectively.

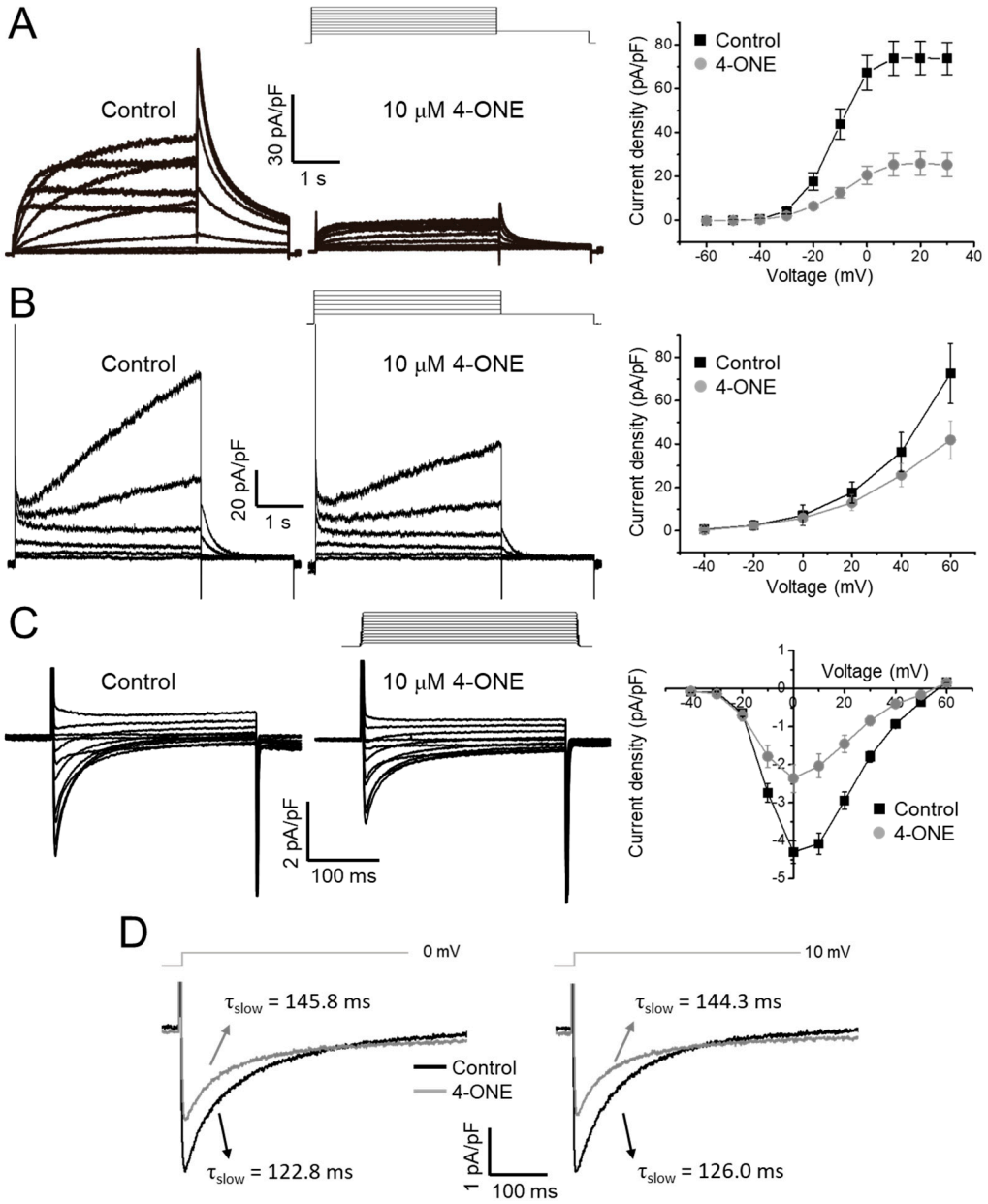


**Figure 4.** Effects of 4-ONE on cardiac ionic currents. (**A**) Human Ether-a-go-go Related Gene (hERG) $K^+$ current ($I_{Kr}$) was inhibited by 4-ONE in hERG-overexpressing HEK cells. $I_{Kr}$ was activated by depolarization from −60 to 30 mV, followed by repolarization of −40 mV evoked the maximum $I_{Kr}$ activity, and the peak $I_{Kr}$ was plotted to I–V relationship curve. (**B**) Slowly activating voltage-dependent $K^+$ current ($I_{Ks}$) was recorded from *KCNQ1/KCNE1*-overexpressing HEK cells. $I_{Ks}$ was activated by depolarization from −40 to 60 mV. The maximum $I_{Ks}$ was analyzed with I–V relationship curve. (**C**) L-type $Ca^{2+}$ current ($I_{Ca,L}$) was activated by applying from −40 to 60 mV of depolarization potentials from −50 mV of holding potential in guinea-pig ventricular myocyte (GPVM). The peak $I_{Ca,L}$ was plotted to I–V relationship curve. (**D**) The decay of $I_{Ca,L}$ was fitted using a double exponential equation. The slow component of time constant ($\tau_{slow}$) of $I_{Ca,L}$ activated by 0 and 10 mV of depolarization potential was indicated.

### *3.3. APD Prolongation and Increased Risk of Arrhythmia by 4-ONE*

The effects of 4-ONE on the cardiac AP were analyzed in GPVM under the current-clamp condition and triggered at 1 Hz. The bath application of 10 μM of 4-ONE markedly prolonged the APD (Figure 5A, B; $APD_{90}$, 309.2 ± 44.50 and 729.4 ± 67.07 ms for control and 4-ONE, respectively, $n$ = 10), which was more prominent than the effect of 100 μM

of 4-HNE, as reported previously [13]. The maximum depolarization speed and total amplitude of APs were not affected by 4-ONE. In addition, the resting membrane potential of GPVMs was not changed (Figure 5B, right).

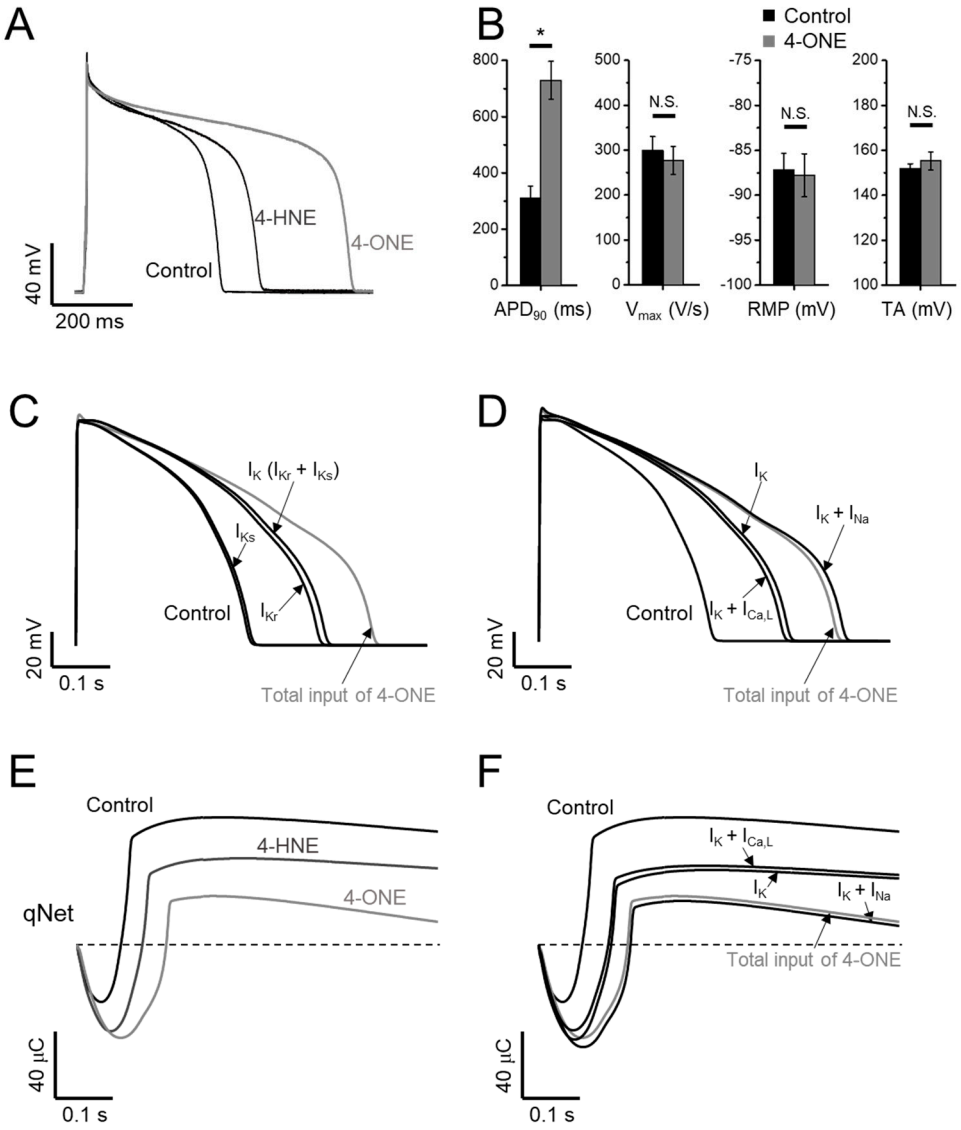


**Figure 5.** Effects of 4-ONE and 4-HNE on guinea-pig action potential (AP) and in silico AP. (**A**,**B**) Representative traces of AP show prolonged AP duration (APD) by 4-HNE (100 μM) and 4-ONE (10 μM) in GPVMs. (**B**) The APs were analyzed by APD at 90% repolarization ($APD_{90}$), maximum overshoot velocity of AP ($V_{max}$), resting membrane potential (RMP), and total amplitude (TA). (**C**–**F**) A CiPAORdv1.0 cell model was used for 4-ONE and 4-HNE simulation. (**C**) The contribution of APD prolongation simulated by $I_K$ ($I_{Kr}$ and $I_{Ks}$) input by 4-ONE. (**D**) The contribution of APD prolongation simulated by $I_{Ca,L}$ and $I_{Na}$ ($I_{NaV}$ and $I_{NaL}$) added to $I_K$ input. (**E**) qNet (net charge carried by total ionic currents) was calculated under 4-HNE and 4-ONE inputs. (**F**) The contribution of qNet simulated by $I_{Ca,L}$ and $I_{Na}$ added to $I_K$ input. All the data were analyzed using paired *t*-tests, where a $p < 0.05$ was considered statistically significant (*).

The CiPA, different from the conventional cardiotoxicity analysis investigating $I_{Kr}$ only, covers the measurements of $I_{Kr}$, $I_{Ca,L}$, $I_{NaV}$, and $I_{NaL}$ for the analysis using the in silico model (CiPAORdv1.0: modified O'Hara–Rudy ventricular myocyte model). Using CiPAORdv1.0, we simulated the AP reflecting the electrophysiological changes induced by 4-ONE treatment (Figure 5C,D). For the calculation of the effects of 4-ONE, the relative

conductance of $I_{Kr}$ and $I_{Ks}$ was decreased to 0.4 and 0.7, respectively. For $I_{Ca,L}$, $I_{NaV}$, and $I_{NaL}$, in addition to the relative conductance, the changes of inactivation kinetics induced by 4-ONE were applied (Table 1). For 4-HNE simulation, the inputs with reduced $I_{Kr}$ and $I_{Ks}$ were applied according to our previous report [13]. The simulated APs revealed markedly prolonged APD by total input of 4-ONE. The decrease in $I_{Kr}$ was more effective than that of $I_{Ks}$ for the APD prolongation. However, it was notable that the modifications of both $K^+$ currents ($I_{Kr}$ and $I_{Ks}$) were insufficient to simulate the change by 4-ONE (Figure 5C). The changes of inward currents ($I_{NaV}$, $I_{NaL}$, and $I_{Ca,L}$) were additionally introduced. While the changes of $I_{Ca,L}$ (slower inactivation and reduced conductance) had an insignificant effect, the increase in $I_{NaL}$ showed a significant additional prolongation of APD (Figure 5D).

The risk of severe arrhythmia, such as Torsades de Pointes (TdP), is evaluated by a novel in silico biomarker, qNet (net charge carried by total ionic currents), proposed from CiPA [24,25]. The decrease in qNet by 10 μM of 4-ONE was more significant than that by 100 μM of 4-HNE (Figure 5E), indicating a higher risk of 4-ONE for arrhythmia induction. In addition, the sufficient reduction of qNet was observed by combining the changes of $I_{Kr}$, $I_{Ks}$, and $I_{Na}$, but not by the simulation using the changes of $I_{Kr}$, $I_{Ks}$, and $I_{Ca,L}$ (Figure 5F), which were consistent with the results of the stepwise simulation of APD change induced by 4-ONE.

## 4. Discussion

Our present study shows prominent cardiac APD prolongation by 4-ONE (10 μM) with multiple effects on the cardiac ion channels. We have previously reported that 100 μM of 4-HNE also induces APD prolongation with the inhibition of $I_{Kr}$ [13]. In addition to the difference in the effective concentrations of the RCS, the APD prolongation and the risk of arrhythmia predicted by CiPA were commonly more prominent with 10 μM of 4-ONE than with 100 μM of 4-HNE (Figure 5). The genetic dysfunction or pharmacological inhibition of $I_{Kr}$ has been regarded as one of the main mechanisms of APD prolongation and EAD. While sharing the inhibitory effect on $I_{Kr}$ with 4-HNE, an additional intriguing finding was the augmentation of $I_{NaL}$ by 4-ONE (Figure 2).

### *4.1. $I_{NaL}$ and Inactivation of $Na_V1.5$*

The very rapid activation of $hNa_V1.5$ is responsible for the fast activation wave and synchronous initiation of cardiac contraction. The inactivation process is also rapid, which prevents wasteful $Na^+$ entry throughout the AP plateau in cardiomyocytes. However, cardiac $I_{NaV}$ also shows residual flow during the sustained depolarization. Although $I_{NaL}$ is relatively negligible to the fast component (0.1%–0.5% of peak $I_{NaV}$), the continuous activity in the AP plateau could contribute to determining the shape and duration of the cardiac AP. Congenital gain-of-function mutations in *SCN5A* coding $hNa_V1.5$ cause LQT-3. LQT-3 patients have a high risk not only for TdP but also for atrial fibrillation [14–16].

$I_{NaL}$ is generally thought to be a persistent opening of the channels modulated either to slow the inactivation or to reopen over the voltage ranges between steady-state activation and inactivation curves, called a "window" potential. An enlargement of the window potential could be induced by the shift of activation or inactivation curves and has been reported as a mechanism of LQT-3 [14,28,29]. In our results, 4-ONE slightly shifted the inactivation curve to the left, implying a narrowed window potential at the relatively positive ranges (Figure 1D, right panel). Considering the voltage difference between the AP plateau (>0 mV, Figure 5) and the window potential under treatment with 4-ONE (below −40 mV, Figure 1E), it is unlikely that the current during the window period of AP could play a significant role for $I_{NaL}$ induction [30].

More importantly, we found that the speed of $hNa_V1.5$ inactivation was slowed by 4-ONE but not by 4-HNE (Figure 2). Cardiac $I_{NaV}$ flows through a channel formed by the α-subunit encoded by *SCN5A*, which alone accounts for major features of $I_{NaV}$ including the fast inactivation. A previous study suggested a structure responsible for the fast inactivation of $I_{NaV}$ resides in IFM motif (isoleucine-phenylalanine-methionine)

on the linker between the third and fourth repeat (DIII–DIV linker) as a "ball" or "lid" and on the bottom of the S4–S5 linker of each repeat (Figure 3E) [31]. In addition to the classical domain for fast inactivation, the perturbation of many locations can destabilize the inactivation and cause pathological $I_{NaL}$ [31–33].

For the mechanisms of $I_{NaL}$ by physiological PTM of $hNa_V1.5$, CaMKII-dependent phosphorylation of $Ser^{571}$ [34] and PKC-dependent phosphorylation of $Ser^{1503}$ [35] have been reported. In addition, the nNOS (NOS1)-dependent S-nitrosylation was suggested, although the precise location of the candidate Cys has not been identified [36]. The non-congenital acquired increase in $I_{NaL}$ is often observed in cardiomyocytes isolated from ischemic hearts and may be due to oxidative stress with increased ROS [37–39]. However, no previous study has paid attention to the modification of $hNa_V1.5$ by 4-ONE that could be abundantly produced by ischemia/reperfusion conditions. In this regard, our present study might suggest a novel mechanism of $I_{NaL}$ induction by ischemia/reperfusion-induced oxidative stress of the heart.

Through the MS/MS analysis, we could identify the binding sites of 4-ONE to $hNa_V1.5$ ($His^{445}$, $His^{472}$, $Lys^{496}$, and $Arg^{878}$). Since the electrophysiological changes by 4-ONE was not reversed by washout with control solution, we carefully suggest that PTM sites revealed by the MS/MS analysis might be the candidate for the slowed inactivation and the increase in $I_{NaL}$ (Figure 3). Although the modified residues are not equivalent to the reported mutations in the congenital LQT-3 patients [14,16,32], those sites are relatively close to the binding sites of a known $I_{NaL}$ activator, veratridine (Figure 3E) [40,41]. The site-directed mutagenesis of $hNa_V1.5$ and the electrophysiological investigation are requested to identify the actual roles of the modified residues in the $I_{NaL}$ and the altered inactivation. Regretfully, we have not conducted the MS/MS analysis with $hNa_V1.5$-HEK cells treated with 4-HNE. Since the treatment with 4-HNE did not induce the functional changes in $I_{NaV}$ inactivation and $I_{NaL}$, the comparative analysis might provide more specific information for the critical residue(s) of $Na_V1.5$ modified by 4-ONE.

### *4.2. Pathophysiological Implication of 4-ONE and $I_{NaL}$*

4-ONE-mediated $I_{NaL}$ induction might have a pathophysiological significance. Increased $I_{NaL}$ in the heart can lead to arrhythmia by prolonging APD in a direct manner and by causing $Ca^{2+}$ overload in an indirect manner. As for the former mechanism, the resurgent $I_{NaL}$ at the repolarization phase of AP interferes with rapid repolarization and can cause EAD-associated arrhythmia. For the latter mechanism, the prolonged APD leads to $Ca^{2+}$ overload by $I_{Ca,L}$ and $Na^+$–$Ca^{2+}$ exchanger, triggering pathological $Ca^{2+}$ release from intracellular $Ca^{2+}$ storing organelles. The $Ca^{2+}$ overload also causes diastolic dysfunction, increased wall stress, and ischemic risk [42]. In this regard, $I_{NaL}$ has been suggested as an attractive therapeutic target to treat arrhythmia, heart failure, and angina. Ranolazine, the most selective clinical $I_{NaL}$ inhibitor, has been used to suppress both arrhythmia events and angina [42,43]. In our result, 4-ONE-mediacted $I_{NaL}$ was effectively reduced by 50 μM ranolazine (Figure 2B), further implying the pathophysiological role of 4-ONE in terms of the cardiac ischemia-associated arrhythmia.

### *4.3. Application of CiPA in Silico Model*

To assess the arrhythmogenic risk of 4-ONE, we applied the CiPA in silico model. The inhibition of $I_{Kr}$ alone could suggest a pathophysiological implication of 4-ONE. Interestingly, the qNet analysis and AP simulations revealed a higher risk of 4-ONE than of 4-HNE, which is due to the $I_{NaL}$ induction. Such insight could not be obtained from the conventional cardiotoxicity test of the $I_{Kr}$ analysis alone, which reflects the strength of CiPA that includes the integrative simulation of the multiple types of cardiac ion channels.

Another interesting feature of the present study was the slowed inactivation and the reduced peak amplitude of $I_{Ca,L}$ by 4-ONE treatment, which was not observed in the previous study of 4-HNE [13]. However, according to the CiPA analysis, the enhanced persistent $Ca^{2+}$ current modulated by the slowed $I_{Ca,L}$ inactivation did not induce significant

changes of the qNet and the simulated APD (Figure 5D,F), which appears to be due to the compensation by the decrease in peak current activation (Figure 4C).

## 5. Conclusions

Using electrophysiological investigation of cardiac ion channel currents, for the first time, we discovered the multichannel effects of 4-ONE, among which the inhibition of $I_{Kr}$ and the induction of $I_{NaL}$ were noteworthy, as confirmed by the qNet reduction indicating arrhythmogenic risk.

**Author Contributions:** Conceptualization, S.-W.C. and S.-J.K.; Methodology, S.-W.C.; Investigation and Data Curation, S.-W.C., M.-Z.Y., N.-K.P. and J.-H.W.; Software, S.-W.C.; Data Analysis, S.-W.C.; Writing—Original Draft Preparation, S.-W.C.; Writing—Review and Editing, S.-J.K.; Funding Acquisition, S.-W.C. and S.-J.K. All authors have read and agreed to the published version of the manuscript.

**Funding:** This research was funded by the National Research Foundation of Korea (NRF) grants funded by the Ministry of Science and ICT of the Korea to S.-J.K. (NRF-2018R1A5A2025964, NRF-2021R1A2C2007243) and S.-W.C. (NRF-2019R1I1A1A01064006).

**Institutional Review Board Statement:** The study was approved by the Institutional Animal Care and Use Committee of Seoul National University (Approval number: SNU-141125-3-1).

**Informed Consent Statement:** Not applicable.

**Data Availability Statement:** Data are contained within the article.

**Acknowledgments:** We greatly appreciate the advice and technical help provided by Jae Beom Youm, Inje University College of Medicine, Busan, Korea.

**Conflicts of Interest:** The authors declare no conflict of interest. The funders had no role in the design of the study; in the collection, analyses, or interpretation of data; in the writing of the manuscript; or in the decision to publish the results.

## References

1. Blair, I.A. Endogenous glutathione adducts. *Curr. Drug. Metab.* **2006**, *7*, 853–872. [CrossRef]
2. Vistoli, G.; De Maddis, D.; Cipak, A.; Zarkovic, N.; Carini, M.; Aldini, G. Advanced glycoxidation and lipoxidation end products (AGEs and ALEs): An overview of their mechanisms of formation. *Free Radic. Res.* **2013**, *47*, 3–27. [CrossRef] [PubMed]
3. Pamplona, R. Advanced lipoxidation end-products. *Chem. Biol. Interact.* **2011**, *192*, 14–20. [CrossRef] [PubMed]
4. Del Rio, D.; Stewart, A.J.; Pellegrini, N. A review of recent studies on malondialdehyde as toxic molecule and biological marker of oxidative stress. *Nutr. Metab. Cardiovasc. Dis.* **2005**, *15*, 316–328. [CrossRef]
5. Kim, C.E.; Lee, S.J.; Seo, K.W.; Park, H.M.; Yun, J.W.; Bae, J.U.; Bae, S.S.; Kim, C.D. Acrolein increases 5-lipoxygenase expression in murine macrophages through activation of ERK pathway. *Toxicol. Appl. Pharmacol.* **2010**, *245*, 76–82. [CrossRef] [PubMed]
6. Lee, S.J.; Kim, C.E.; Yun, M.R.; Seo, K.W.; Park, H.M.; Yun, J.W.; Shin, H.K.; Bae, S.S.; Kim, C.D. 4-Hydroxynonenal enhances MMP-9 production in murine macrophages via 5-lipoxygenase-mediated activation of ERK and p38 MAPK. *Toxicol. Appl. Pharmacol.* **2010**, *242*, 191–198. [CrossRef] [PubMed]
7. Ma, H.; Guo, R.; Yu, L.; Zhang, Y.; Ren, J. Aldehyde dehydrogenase 2 (ALDH2) rescues myocardial ischaemia/reperfusion injury: Role of autophagy paradox and toxic aldehyde. *Eur. Heart J.* **2011**, *32*, 1025–1038. [CrossRef] [PubMed]
8. Barrera, G.; Gentile, F.; Pizzimenti, S.; Canuto, R.A.; Daga, M.; Arcaro, A.; Cetrangolo, G.P.; Lepore, A.; Ferretti, C.; Dianzani, C.; et al. Mitochondrial dysfunction in cancer and neurodegenerative diseases: Spotlight on fatty acid oxidation and lipoperoxidation products. *Antioxidants* **2016**, *5*, 7. [CrossRef] [PubMed]
9. Gianazza, E.; Brioschi, M.; Fernandez, A.M.; Banfi, C. Lipoxidation in cardiovascular diseases. *Redox Biol.* **2019**, *23*, 101119. [CrossRef] [PubMed]
10. Asselin, C.; Ducharme, A.; Ntimbane, T.; Ruiz, M.; Fortier, A.; Guertin, M.C.; Lavoie, J.; Diaz, A.; Levy, E.; Tardif, J.C.; et al. Circulating levels of linoleic acid and HDL-cholesterol are major determinants of 4-hydroxynonenal protein adducts in patients with heart failure. *Redox Biol.* **2014**, *2*, 148–155. [CrossRef]
11. Giam, B.; Chu, P.Y.; Kuruppu, S.; Smith, A.I.; Horlock, D.; Kiriazis, H.; Du, X.J.; Kaje, D.M.; Rajapakse, N.W. N-acetylcysteine attenuates the development of cardiac fibrosis and remodeling in a mouse model of heart failure. *Physiol. Rep.* **2016**, *4*, e12757. [CrossRef]
12. Gupta, R.C.; Singh-Gupta, V.; Zhang, K.F.; Xu, J.; Sabbah, H.N. Elamipretide (Bendavia (TM)) restores 4-hydroxy-2-nonenal protein adducts and aldehyde dehydrogenase-2 activity and mRNA expression in left ventricular myocardium of dogs with advanced heart failure. *Circulation* **2016**, *134*, A12949.

13. Choi, S.W.; Choi, S.W.; Jeon, Y.K.; Moon, S.H.; Zhang, Y.H.; Kim, S.J. Suppression of hERG K(+) current and cardiac action potential prolongation by 4-hydroxynonenal via dual mechanisms. *Redox Biol.* **2018**, *19*, 190–199. [CrossRef] [PubMed]
14. Ruan, Y.; Liu, N.; Priori, S.G. Sodium channel mutations and arrhythmias. *Nat. Rev. Cardiol.* **2009**, *6*, 337–348. [CrossRef] [PubMed]
15. Darbar, D.; Kannankeril, P.J.; Donahue, B.S.; Kucera, G.; Stubblefield, T.; Haines, J.L.; George, A.L.; Roden, D.M. Cardiac sodium channel (SCN5A) variants associated with atrial fibrillation. *Circulation* **2008**, *117*, 1927–1935. [CrossRef] [PubMed]
16. Wilde, A.M.; Amin, A.S. Clinical spectrum of SCN5A mutations: Long QT syndrome, Brugada syndrome, and cardiomyopathy. *JACC Clin. Electrophysiol.* **2018**, *4*, 569–579. [CrossRef] [PubMed]
17. Ju, Y.K.; Saint, D.A.; Gage, P.W. Hypoxia increases persistent sodium current in rat ventricular myocytes. *J. Physiol.* **1996**, *497*, 337–347. [CrossRef]
18. Undrovinas, A.I.; Maltsev, V.A.; Sabbah, H.N. Repolarization abnormalities in cardiomyocytes of dogs with chronic heart failure: Role of sustained inward current. *Cell Mol. Life Sci.* **1999**, *55*, 494–505. [CrossRef]
19. Valdivia, C.R.; Chu, W.W.; Pu, J.L.; Foell, J.D.; Haworth, R.A.; Wolff, M.R.; Kamp, T.J.; Makielski, J.C. Increased late sodium current in myocytes from a canine heart failure model and from failing human heart. *J. Mol. Cell. Cardiol.* **2005**, *38*, 475–483. [CrossRef]
20. Zhang, W.H.; Liu, J.; Xu, G.; Yuan, Q.; Sayre, L.M. Model studies on protein side chain modification by 4-oxo-2-nonenal. *Chem. Res. Toxicol.* **2003**, *16*, 512–523. [CrossRef]
21. Doorn, J.A.; Petersen, D.R. Covalent adduction of nucleophilic amino acids by 4-hydroxynonenal and 4-oxononenal. *Chem. Biol. Interact.* **2003**, *143*, 93–100. [CrossRef]
22. Lee, S.H.; Blair, I.A. Characterization of 4-oxo-2-nonenal as a novel product of lipid peroxidation. *Chem. Res. Toxicol.* **2000**, *13*, 698–702. [CrossRef] [PubMed]
23. Taylor-Clark, T.E.; McAlexander, M.A.; Nassenstein, C.; Sheardown, S.A.; Wilson, S.; Thornton, J. Relative contributions of TRPA1 and TRPV1 channels in the activation of vagal bronchopulmonary C-fibres by the endogenous autacoid 4-oxononenal. *J. Physiol.* **2008**, *586*, 3447–3459. [CrossRef] [PubMed]
24. Li, Z.; Ridder, B.J.; Han, X.; Wu, W.W.; Sheng, J.; Tran, P.N.; Wu, M.; Randolph, A.; Johnstone, R.H.; Mirams, G.R.; et al. Assessment of an in silico mechanistic model for proarrhythmia risk prediction under the CiPA initiative. *Clin. Pharmacol. Ther.* **2019**, *105*, 466–475. [CrossRef] [PubMed]
25. Dutta, S.; Chang, K.C.; Beattie, K.A.; Sheng, J.; Tran, P.N.; Wu, W.W.; Wu, M.; Strauss, D.G.; Colatsky, T.; Li, Z. Optimization of an in silico cardiac cell model for proarrhythmia risk assessment. *Front. Physiol.* **2017**, *8*, 616. [CrossRef]
26. Jian, W.; Lee, S.H.; Mesaros, C.; Oe, T.; Silva Elipe, M.V.; Blair, I.A. A novel 4-oxo-2(E)-nonenal-derived endogenous thiadiazabicyclo glutathione adduct formed during cellular oxidative stress. *Chem. Res. Toxicol.* **2007**, *20*, 1008–1018. [CrossRef]
27. Doorn, J.A.; Petersen, D.R. Covalent modification of amino acid nucleophiles by the lipid peroxidation products 4-hydroxy-2-nonenal and 4-oxo-2-nonenal. *Chem. Res. Toxicol.* **2002**, *15*, 1445–1450. [CrossRef]
28. Clancy, C.E.; Tateyama, M.; Kass, R.S. Insights into the molecular mechanisms of bradycardia-triggered arrhythmias in long QT-3 syndrome. *J. Clin. Investig.* **2002**, *110*, 1251–1262. [CrossRef]
29. Tian, X.L.; Yong, S.L.; Wan, X.; Wu, L.; Chung, M.K.; Tchou, P.J.; Rosenbaum, D.S.; Van Wagoner, D.R.; Kirsch, G.E.; Wang, Q. Mechanisms by which SCN5A mutation N1325S causes cardiac arrhythmias and sudden death in vivo. *Cardiovasc. Res.* **2004**, *61*, 256–267. [CrossRef]
30. Kistamás, K.; Hézső, T.; Horváth, B.; Nánási, P.P. Late sodium current and calcium homeostasis in arrhythmogenesis. *Channels* **2021**, *15*, 1–19. [CrossRef]
31. Mangold, K.E.; Brumback, B.D.; Angsutararux, P.; Voelker, T.L.; Zhu, W.; Kang, P.W.; Moreno, J.D.; Silva, J.R. Mechanisms and models of cardiac sodium channel inactivation. *Channels* **2017**, *11*, 517–533. [CrossRef] [PubMed]
32. Veerman, C.C.; Wilde, A.A.M.; Lodder, E.M. The cardiac sodium channel gene SCN5A and its gene product NaV1.5: Role in physiology and pathophysiology. *Gene* **2015**, *573*, 177–187. [CrossRef] [PubMed]
33. Wang, Q.; Chen, S.; Chen, Q.; Wan, X.; Shen, J.; Hoeltge, G.A.; Timur, A.A.; Keating, M.T.; Kirsch, G.E. The common SCN5A mutation R1193Q causes LQTS-type electrophysiological alterations of the cardiac sodium channel. *J. Med. Genet.* **2004**, *41*, e66. [CrossRef] [PubMed]
34. Howard, T.; Greer-Short, A.; Satroplus, T.; Patel, N.; Nassal, D.; Mohler, P.J.; Hund, T.J. CaMKII-dependent late Na+ current increases electrical dispersion and arrhythmia in ischemia-reperfusion. *Am. J. Physiol. Heart Circ. Physiol.* **2018**, *315*, H794–H801. [CrossRef]
35. Hallaq, H.; Wang, D.W.; Kunic, J.D.; George, A.L., Jr.; Wells, K.S.; Murray, K.T. Activation osf protein kinase C alters the intracellular distribution and mobility of cardiac Na+ channels. *Am. J. Physiol. Heart Circ. Physiol.* **2012**, *302*, H782–H789. [CrossRef] [PubMed]
36. Ueda, K.; Valdivia, C.; Medeiros-Domingo, A.; Tester, D.J.; Vatta, M.; Farrugia, G.; Ackerman, M.J.; Makielski, J.C. Syntrophin mutation associated with long QT syndrome through activation of the nNOS-SCN5A macromolecular complex. *Proc. Natl. Acad. Sci. USA* **2008**, *105*, 9355–9360. [CrossRef] [PubMed]
37. Tang, Q.; Ma, J.; Zhang, P.; Wan, W.; Kong, L.; Wu, L. Persistent sodium current and Na+/H+ exchange contributes to the augmentation of the reverse Na+/Ca2+ exchange during hypoxia or acute ischemia in ventricular myocytes. *Pflugers Arch.* **2012**, *463*, 513–522. [CrossRef]

38. Shimoda, L.A.; Polak, J. Hypoxia. 4. Hypoxia and ion channel function. *Am. J. Physiol. Cell Physiol.* **2011**, *300*, C951–C967. [CrossRef] [PubMed]
39. Ahern, G.P.; Hsu, S.F.; Klyachko, V.A.; Jackson, M.B. Induction of persistent sodium current by exogenous and endogenous nitric oxide. *J. Biol. Chem.* **2000**, *275*, 28810–28815. [CrossRef]
40. Denac, H.; Mevissen, M.; Scholtysik, G. Structure, function and pharmacology of voltage-gated sodium channels. *Naunyn Schmiedebergs Arch. Pharmacol.* **2000**, *362*, 453–479. [CrossRef]
41. Stevens, M.; Peigneur, S.; Tytgat, J. Neurotoxins and their binding areas on voltage-gated sodium channels. *Front. Pharmacol.* **2011**, *2*, 71. [CrossRef] [PubMed]
42. Sossalla, S.; Maier, L.S. Role of ranolazine in angina, heart failure, arrhythmias, and diabetes. *Pharmacol. Therapeutics* **2012**, *133*, 311–323. [CrossRef] [PubMed]
43. Gupta, T.; Khera, S.; Kolte, D.; Aronow, W.S.; Iwai, S. Antiarrhythmic properties of ranolazine: A review of the current evidence. *Int. J. Cardiol.* **2015**, *187*, 66–74. [CrossRef] [PubMed]